Photoelectron angular distributions from two-photon ionization of atoms near ionization threshold

Lihua Bai (白丽华)*, Tingting Cui (崔婷婷), Yuheng Liu (刘宇恒), Yan Wang (王 燕), Dongmei Deng (邓冬梅), and Jihui Tao (陶继辉)

Department of Physics, Shanghai University, Shanghai 200444, China

**Corresponding author: lhbai@163.com*

Received August 2, 2010; accepted September 21, 2010; posted online January 1, 2011

Photoelectron angular distributions (PADs) from two-photon ionization of atoms in linearly polarized strong laser fields are obtained in accordance with the nonperturbative quantum scattering theory. We also study the influence of laser wavelength on PADs. For two-photon ionization very close to the ionization threshold, most of the ionized electrons are vertically ejected to the laser polarization. PADs from two-photon ionization of atoms are determined by the second order generalized phased Bessel function at which the ponderomotive parameter plays a key role. In terms of dependence of PADs on laser wavelength, corresponding variations for the ponderomotive parameter are demonstrated.

OCIS codes: 020.4180, 020.2649.

doi: 10.3788/COL201109.010203.

Both theoretical and experimental studies on photoelectron angular distributions (PADs) from the above-threshold ionization (ATI) of atoms have been exceedingly significant[1−10]. Detailed studies on PADs have resulted in substantial knowledge advancements in terms of atomic dynamics in strong fields. Comparisons between theoretical results and experimental observations have offered stringent tests on numerous extant strong-field ionization theories.

Dodhy *et al*. have measured PADs of Cs and Rb atoms for near-threshold two-photon ionization[11]. Focusing on PADs in a region very close to the ionization threshold, they have observed that these PADs exhibit lower order ionization peaks. They have also reported that the ratios of ionization rate of $\phi_{\rm f} = 90^\circ$ to that of $\phi_{\rm f} = 0^\circ$ in both Cs and Rb atoms decrease with the decline laser wavelength, where $\phi_{\rm f}$ is the angle between the polarization of the laser and the fixed detection of photoelectrons. Furthermore, they have found that such ratio is larger in Rb atom compared with that in Cs atom despite the approximately same values of photoelectron energy.

In this letter, we consider the nonperturbative scattering theory proposed by Guo, Aberg, and Crasemann (GAC theory) in studying two-photon ionization of Rb and Cs atoms in intense laser fields[12]. The GAC theory[12] of photoionization in intense fields has been proven successful in explaining strong-field phenomena. As prescribed by this theory, free electrons moving in electromagnetic fields are considered as intermediate states whereas the final state of the ionized electron is an electron-photon plane wave. This theory has allowed for the interpretation[9] of the angular splitting in experiment[13]. In addition, this theory has successfully explained the recent research on the jet-like structure in PADs, as observed by Nandor *et al*.[14]. Based on previous reports, PADs can be determined by a generalized phased Bessel (GPB) function at which the jets are caused by the corresponding maximum of the same function[15]. Thereafter, the scaling law of PADs has been established[16]. The advantage of GAC theory lies in its simplicity and capability to produce a PAD pattern similar to those from experimental observations.

In this letter, PADs from two-photon ionization (for the first order ATI peak) of Cs and Rb atoms near the ionization threshold in strong linearly polarized laser fields are determined in accordance with GAC theory. The influence of laser wavelength on the PADs is investigated. Findings show that 1) the PADs exhibit a main lobe along the polarized direction and a central jet perpendicular to the polarized direction, especially for near-threshold two-photon ionization, after which the central jet becomes the main structure of PADs; 2) the ratio of ionization rates, $\phi_{\rm f} = 90^\circ$ (central jet) to $\phi_{\rm f} = 0^\circ$ (main lobe), decreases as the laser wavelength decreases; and 3) the intensity ratio (i.e., central jet to main lobe) is larger in Rb than in Cs despite the approximately same values of photoelectron energy, which is in agreement with the study of Dodhy *et al*.[11]. For Cs and Rb atoms, PADs are particularly sensitive to laser frequency, such that PADs change dramatically with the minimal change in laser frequency. Notably, the central jet became the main structure of PADs in the close vicinity of the threshold. A bell shape with the maximum point perpendicular to the laser polarization is demonstrated.

The differential ionization-rate formula is given as[17]

$$\frac{{\rm d}^2W}{{\rm d}^2\Omega_{\mathbf{P}_{\rm f}}}\Big|_j = \frac{e^2\omega^{9/2}}{(2m_{\rm e})^{1/2}(2\pi)^5}(j-\varepsilon_{\rm b}-u_{\rm p})^{1/2} \times (j-u_{\rm p})^2\sum_{q>\varepsilon_{\rm b}}(u_{\rm p}-j+q)\times\int {\rm d}^2\Omega_{\mathbf{k}'} \left|\Phi_{\rm i}(\mathbf{P}_{\rm f}-q\mathbf{k}+\mathbf{k}')\right|^2\times\left|\chi_q(\mathbf{P}_{\rm f},\mathbf{k}')\right|^2, \quad (1)$$

where ${\rm d}\Omega_{\mathbf{P}_{\rm f}} = \sin\theta_{\rm f}{\rm d}\theta_{\rm f}{\rm d}\phi_{\rm f}$ is the differential solid angle of the final photoelectron; $\theta_{\rm f}$ and $\phi_{\rm f}$ are the scattering angle and the azimuth angle; $\mathbf{P}_{\rm f}$ is the final momentum of photoelectron; j is the number of the absorbed photons in the ionization process, $j = 2$ corresponds to a two-photon ionization; q is the overall transferred photon number; e is the charge of electron; $m_{\rm e}$ is the electron

rest mass; ω is the frequency of the laser field; $\mathbf{k}$ and $\mathbf{k}'$ are the wave vectors of the laser field and spontaneously emitted light, respectively; and $\varepsilon_{\rm b} = E_{\rm b}/\omega$ is the atomic binding energy in units of the laser photon energy. The ponderomotive parameter $u_{\rm p}$ is defined as

$$u_{\rm p} = \frac{e^2\Lambda^2}{m_{\rm e}\omega}, \tag{2}$$

where 2Λ is the classical amplitude of the laser field. $\Phi_{\rm i}(\mathbf{P}_{\rm f} - q\mathbf{k} + \mathbf{k}')$ is the Fourier transform of the initial wave function. Then, $\chi_q(\mathbf{P}_{\rm f}, \mathbf{k}')$ is defined as

$$\begin{aligned}\chi_q(\mathbf{P}_{\rm f}, \mathbf{k}') = \frac{1}{\omega}\chi_{-j}(Z,\eta) \sum_{j'=-\infty}^{\infty} \frac{1}{u_{\rm p} - j'}\chi_{-j'}(Z,\eta) \\ \times [-(\mathbf{P}_{\rm f} + (j - q - u_{\rm p})\mathbf{k}) \cdot \boldsymbol{\varepsilon}'^{*} X_{q-j+j'}(Z_{\mathbf{k}'}) \\ + e\Lambda\boldsymbol{\varepsilon}^{*} \cdot \boldsymbol{\varepsilon}'^{*} X_{q-j+j'+1}(Z_{\mathbf{k}'}) \\ + e\Lambda\boldsymbol{\varepsilon} \cdot \boldsymbol{\varepsilon}'^{*} X_{q-j+j'-1}(Z_{\mathbf{k}'})].\end{aligned} \tag{3}$$

The GPB function is

$$\chi_{-j}(Z,\eta) = \sum_{s=-\infty}^{\infty} X_{-j+2s}(Z) X_{-s}(\eta), \tag{4}$$

where s is the order of the GPB function, and $X_n(Z)$ is the phased Bessel function[18].

The arguments of the GPB function are as follows:

$$\begin{aligned} Z_{\rm f} = 2\frac{|e|\,\Lambda}{m_{\rm e}\omega}\mathbf{P}_{\rm f} \cdot \boldsymbol{\varepsilon}, \quad Z_{\mathbf{k}'} = 2\frac{|e|\,\Lambda}{m_{\rm e}\omega}\mathbf{k}' \cdot \boldsymbol{\varepsilon}, \\ Z = Z_{\rm f} + Z_{\mathbf{k}'}, \qquad \eta = \frac{1}{2}u_{\rm p}\cos\xi, \end{aligned} \tag{5}$$

where ξ monitors the polarization degree, such that $\xi = 0$ denotes linear polarization and $\xi = \pi/2$ denotes circular polarization. In Eq. (3), $\boldsymbol{\varepsilon}$ is the polarization vector of laser light, $\boldsymbol{\varepsilon}'$ is the polarization vector of the spontaneously emitted light, and $\boldsymbol{\varepsilon}'^{*}$ is the conjugate of $\boldsymbol{\varepsilon}'$. In long-wavelength approximation (LWA), if $\mathbf{k}' \ll \mathbf{P}_{\rm f}$, then $Z_{\mathbf{k}'} \ll Z_{\mathbf{f}}$, which leads to $Z \cong Z_{\mathbf{f}}$.

PAD corresponds to the ionization rate for different azimuths at a fixed scattering angle. Most experimental observations were performed in the polarization plane defined by $\theta_{\rm f} = \pi/2$. PAD was obtained according to Eq. (1) by setting the scattering angle ($\theta_{\rm f}$) to $\pi/2$ and by varying the azimuth angle ($\phi_{\rm f}$) from 0° to 180° with a step size of 6°. In our calculations, the binding energies of Cs and Rb atoms were 3.894 and 4.177 eV, respectively.

In general, PADs in linearly polarized laser fields exhibit a remarkable structure. Aside from main lobes along the direction of laser polarization, prominent electron jets are also emitted from the waist between the main lobes. In PADs from two-photon ionization, there is always one central jet structure. The ratio of the height of the central jet to that of the main lobe varies with laser frequency. Thereafter, the influence of the laser wavelength can be determined.

The influence of the laser wavelength can be demonstrated in many aspects. For example, the PADs and electron kinetic spectrum vary with laser wavelength. In this letter, the laser wavelength was set to vary from 420 to 560 nm for the Cs atom and from 400 to 530 nm for the Rb atom. Accordingly, two photons were absorbed to form the first ATI peak.

We first showed the calculated PADs of a Rb atom from a two-photon ATI. In our calculations, the laser intensity was 1×10^{10} W/cm^2 and the laser wavelength varied from 400 to 530 nm; this was conducted to ensure the ionization process in the domain between the one-photon and two-photon ionization thresholds. The PADs are illustrated in Fig. 1.

Three notable observations were gathered. 1) Each of the plots shows the main lobe to be along the laser polarization and the central jet vertical to the laser polarization. 2) The ratio of the height of the central jet to that of the main lobe varies with laser wavelength in the domain very close to the two-photon threshold, and the central jet becomes the dominant structure in PADs. In Fig. 1(a), for a laser wavelength of 400 nm, the height of the central jet is far lower than that of the main lobe, the ratio of which is about 0.39. As the laser wavelength increases, the central jet becomes excessively higher (Fig. 1(b)). For the laser wavelength of 420 nm, this ratio is about 0.56. Based on Figs. 1(c) and (d), for laser wavelengths of 490 and 530 nm, respectively, the central jet becomes the dominant structure in PADs further as laser wavelength is increased, indicating that most ionized electrons are ejected vertically to the laser polarization. The ratio is much greater than 1.0; that is, it is 6.58 in Fig. 1(c) and approximately 50 in Fig. 1(d). In addition, in Fig. 1(d), with the frequency very close to the two-photon threshold, the PADs are presented as bell-shaped, demonstrating the so-called threshold effect by Reichle *et al.*[19]. 3) The ratio of the ionization rate for the central jet to that of the main lobe decreases as the laser wavelength decreases, which agrees well with the study of Dodhy *et al.*[11]

In Fig. 2, we show the calculated PADs of Cs atoms from a two-photon ATI. In our calculations, the laser intensity was 1×10^{10} W/cm^2 and the laser wavelength varied from 420 to 560 nm; this was conducted to ensure

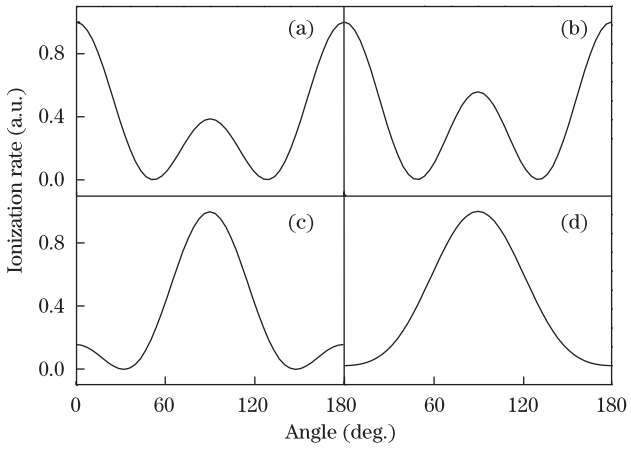

Fig. 1. PADs from two-photon ionization of a Rb atom at the fixed laser intensity of 1×10^{10} W/cm^2 for different central laser wavelengths: (a) 400, (b) 420, (c) 490, and (d) 530 nm. For convenience in comparison, each plot is normalized by the maximum of PAD.

the ionization process in the domain between the one-photon and two-photon ionization thresholds.

We observed two prominent features from Fig. 2. 1) Each plot shows the main lobe to be along the laser polarization and the central jet vertical to the laser polarization. 2) The ratio of the height of central jet to that of the main lobe varies with laser wavelength. For a laser wavelength of 420 nm (Fig. 2(a)), the height of the central jet is far lower than that of the main lobe; the ratio is about 0.34. As the laser wavelength increases (i.e., 440 nm), the central jet excessively higher (Fig. 2(b)), such that the ratio of the height of central jet to that of the main lobe is about 0.46. For laser wavelengths of 520 and 560 nm (Figs. 2(c) and (d), respectively), the central jet becomes the dominant structure in PADs. This indicates that most ionized electrons are ejected vertically to the laser polarization. The ratio was notably greater than 1.0; that is, it was 4.6 and even higher (Figs. 2(c) and (d), respectively).

For PADs at which the height of the central jet was smaller than that of the main lobe, the corresponding ratio on intensity was larger in Rb than in Cs despite the presence of photoelectron with similar energies; such finding is consistent with the study of Dodhy *et al.*[11] For example, in Figs. 1(a) and 2(a), the values of photoelectron energy are approximately similar for both cases; the ratio is 0.39 in Fig. 1(a) for the Rb atom and 0.34 in Fig. 2(a) for Cs atoms. A similar situation could be observed when comparing Figs. 1(b) and 2(b).

The PADs in the two-photon ionization were determined by the second-order GPB function, $\chi_{-2}(Z_{\rm f},\eta)$, and the central jet in PADs was caused by the maximum of the GPB function in the domain of the variable[10]. The ratio of the height of the central jet to that of the main lobe was determined by $|\chi_{-2}(0,\eta)/\chi_{-2}(Z_{\rm f\,max},\eta)|^2$, where $\chi_{-2}(0,\eta)$ denotes the central jet in PADs and $\chi_{-2}(Z_{\rm f\,max},\eta)$ corresponds to the detachment rate along the laser polarization. Since $Z_{\rm f\,max}$ and η vary with the laser frequency, the influence of laser frequency on PADs can be reflected by altering the jet structure and main lobe.

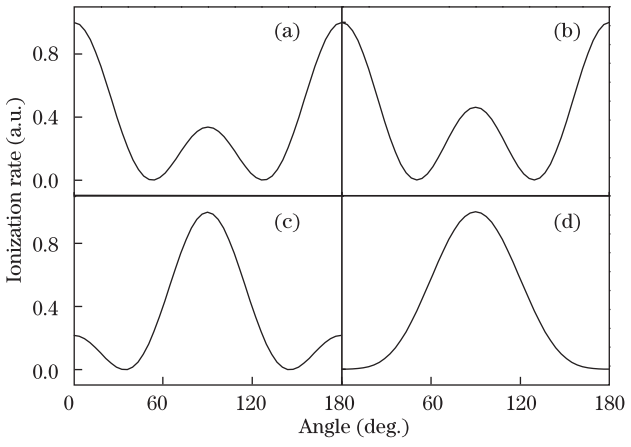

Fig. 2. PADs from two-photon ionization of Cs atoms at the fixed laser intensity of 1×10^{10} W/cm^2 for different central laser wavelengths: (a) 420, (b) 440, (c) 520, and (d) 560 nm. For convenience in comparison, each plot is normalized by the maximum of PAD.

The laser frequency influenced the PADs through the variations in the ponderomotive parameter $u_{\rm p}$. The ponderomotive shift $U_{\rm p}$ can be written as

$$U_{\rm p} = u_{\rm p}\omega = \frac{2\pi e^2 I}{m_{\rm e}\omega^2},$$

which varies with the laser frequency (I is the laser intensity). A lower laser frequency corresponds to a larger ponderomotive shift. The energy conservation in the overall process shows the final kinetic energy of the electron after two-photon ionization, satisfying

$$E_{\mathbf{k}} \equiv \frac{\mathbf{P}_{\rm f}^2}{2m_{\rm e}} = 2\omega - U_{\rm p} - E_{\rm b} = 2\omega - u_{\rm p}\omega - E_{\rm b}. \quad (6)$$

Equation (6) suggests that the final kinetic energy decreases with the decrease in laser frequency. Therefore, by changing the ponderomotive parameter $u_{\rm p}$, the laser frequency then affects the ponderomotive shift $U_{\rm p}$. Consequently, the final kinetic energy of emitted electrons $E_{\mathbf{k}}$ and PADs vary with laser frequency.

Essentially, the ponderomotive parameter $u_{\rm p}$ varies with laser wavelength, the main factor that alters the values of the two variables of the GPB function and then affects PADs. The variables of the GPB function after two-photon ionization can be written as

$$Z_{\rm f} = \sqrt{8u_{\rm p}(2-u_{\rm p}-\varepsilon_{\rm b})}\cos\phi_{\rm f} = Z_{\rm f\,max}\cos\phi_{\rm f}. \quad (7)$$

The corresponding value of $Z_{\rm f}$ that leads to $\chi_{-2}(Z_{\rm f},\eta) = 0$ is denoted by $Z_{\rm f0}$. The parameter $u_{\rm p}$ varies with laser frequency. Subsequently, the values of $Z_{\rm f\,max}$ and η would also change. Variations in variables alter the value of $Z_{\rm f0}$ and the ratio of $\chi_{-2}(0,\eta)/\chi_{-2}(Z_{\rm f\,max},\eta)$, an indication of the influence of laser wavelength.

The laser wavelength affects PADs, ionization, and other physical processes along the strong field through the influence on the variables of the GPB function by means of the ponderomotive parameter. This indicates that the ponderomotive parameter is a key parameter in the strong fields.

In conclusion, in accordance with the nonperturbative quantum scattering theory, the PADs from two-photon ionization of Rb and Cs atoms in strong linearly polarization laser fields are presented. The PADs have exhibited a main lobe along the polarization direction and a central jet perpendicular to the polarized direction, especially for the near-threshold two-photon ionization, after which the central jet becomes the main structure of the PADs. The PADs from the two-photon ionization of atoms are determined by the second-order GPB function at which the ponderomotive parameter plays a key role. In terms of dependence of PADs on laser wavelength, corresponding variations for the ponderomotive parameter have been demonstrated.

This work was supported by the National Natural Science Foundation of China under Grant Nos. 60908006, 10804067, and 60407007.

References

1. R. Freeman, T. McIlrath, P. Bucksbaum, and M. Bashkansky, Phys. Rev. Lett. **57,** 3156 (1986).

2. M. Bashkansky, P. Bucksbaum, and D. Schumacher, Phys. Rev. Lett. **60,** 2458 (1988).
3. S. Basile, F. Trombetta, and G. Ferrante, Phys. Rev. Lett. **61,** 2435 (1988).
4. Y. Li, J. Liu, R. Fan, L. Ren, and R. Ma, Chinese J. Lasers (in Chinese) **36,** 2865 (2009).
5. Y. Li, R. Fan, J. Liu, L. Ren, and R. Ma, Acta Opt. Sin. (in Chinese) **30,** 551 (2010).
6. J. Zhang, X. Feng, Z. Xu, and D. Guo, Phys. Rev. A **69,** 043409 (2004).
7. S. Dionissopoulou, T. Mercouris, A. Lyras, and C. Nicolaides, Phys. Rev. A **55,** 4397 (1997).
8. V. Schvja, T. Lang, and H. Helm, Phys. Rev. A **57,** 3692 (1998).
9. D. Guo and G. Drake, Phys. Rev. A **45,** 6622 (1992).
10. J. Zhang, S. Li, and Z. Xu, Phys. Rev. A **69,** 053410 (2004).
11. A. Dodhy, R. Compton, and J. Stockdale, Phys. Rev. Lett. **54,** 422 (1985).
12. D. Guo, T. Aberg, and C. Crasemann, Phys. Rev. A **40,** 4997 (1989).
13. P. H. Bucksbaum, D. W. Schumacher, and M. Bashkansky, Phys. Rev. Lett. **61,** 1182 (1988).
14. M. Nandor, M. Walker, and L. Woerkom, J. Phys. B: At. Mol. Opt. Phys. **31,** 4617 (1998).
15. J. Zhang, W. Zhang, Z. Xu, X. Li, P. Fu, D. Guo, and R. Freeman, J. Phys. B: At. Mol. Opt. Phys. **35,** 4809 (2002).
16. D. Guo, J. Zhang, Z. Xu, X. Li, P. Fu, and R. Freeman, Phys. Rev. A **68,** 043404 (2003).
17. J. Gao, D. Guo, and Y. Wu, Phys. Rev. A **61,** 043406 (2000).
18. X. Hu, H. Wang, and D. Guo, Can. J. Phys. **86,** 863 (2008).
19. R. Reichle, H. Helm, and I. Kiyan, Phys. Rev. Lett. **87,** 243001 (2001).